Simulation of spin field effect transistors: Effects of tunneling and spin relaxation on performance

Yunfei Gao,[1,a)] Tony Low,[1] Mark S. Lundstrom,[1] and Dmitri E. Nikonov[2]
[1]*Department of Electrical and Computer Engineering, Purdue University, West Lafayette, Indiana 47906, USA*
[2]*Components Research, Intel Corporation, 2200 Mission College Blvd., Santa Clara, California 95052, USA*

(Received 1 February 2010; accepted 31 August 2010; published online 18 October 2010)

A numerical simulation of spin-dependent quantum transport for a spin field effect transistor is implemented in a widely used simulator, nanoMOS. This method includes the effect of both spin scattering in the channel and the tunneling barrier between the source/drain and the channel. Accounting for these factors permits setting more realistic performance limits for the transistor, especially the magnetoresistance, which is found to be lower compared to earlier predictions. The interplay between tunneling and spin scattering is elucidated by numerical simulation. Insertion of the tunneling barrier leads to an increased magnetoresistance. Simulations are used to explore the tunneling barrier design issues. © *2010 American Institute of Physics*. [doi:10.1063/1.3496666]

I. INTRODUCTION

Spin-based logic is currently being explored as a potential beyond-complementary metal-oxide-semiconductor (CMOS) computing technologies,[1] which are presently being considered to supplement CMOS field effect transistors (FETs) in microprocessors. Vigorous research in spintronic devices has been carried out over the last two decades[2–4] and has resulted in demonstration of two-terminal giant magnetoresistance (MR),[5,6] tunneling MR (TMR) (Ref. 7) devices, and TMR devices switched by spin transfer torque.[8] Such devices have been commercialized in magnetic hard drives and magnetic random access memories and have a great impact on everyday life. The question arises now whether there is a spintronic device capable of similar success in logic applications.

One of the candidates is the spinFET first proposed by Sugahara and Tanaka,[9] a three-terminal device that utilizes ferromagnetic (FM) contacts in the source and drain as spin injector and detector. The spinFET is essentially a combination of two Schottky barrier (SB) metal-oxide-semiconductor field-effect transistors (MOSFETs), each implemented by carriers with a certain spin state (e.g., one up-spin and one down-spin). The transport channels for up-spin and down-spin electrons (or holes) are independent if no spin scattering occurs but they become interconnected if spin-flip processes happen. The semiconductor channel makes the spinFET compatible with the modern CMOS technology. Relatively small spin orbit coupling and negligible hyperfine interaction give electrons a long spin lifetime in silicon,[10] which makes it a good candidate for the channel material. However, spinFETs are also envisioned with germanium or III-V semiconductor channels. Due to the exchange splitting between the up-spin and down-spin bands in the FM contacts, the up-spin and down-spin carriers experience different barriers between the contacts and the channel. The gate controls the width of the SBs and the electrostatic potential in the channel. The magnetizations of the source and drain can be switched to be parallel or antiparallel to obtain low or high resistance between these contacts, respectively, similar to a magnetic tunnel junctions (MTJs).[7,11] Therefore, the current flow is controlled by the gate and drain bias, and also by the direction of the contacts' magnetization. The switching of magnetization can be performed, for example, by spin transfer torque of the flowing current. The spinFET must be distinguished from the spin modulator based on spin precession, the original spintronic device proposed by Datta and Das.[12] We will not consider this device here, though some later publications called it "spinFET."

The MR ratio, which is a key device performance metric of a spintronic device, is defined via the resistances for parallel (R_P) and antiparallel (R_{AP}) contact magnetization configurations as follows $MR=(R_{AP}-R_P)/R_P$. The identical quantity (provided a fixed voltage is applied) is the magnetocurrent ratio $MC=(I_P-I_{AP})/I_{AP}$. In order to improve MR, high spin polarization in both source and drain contacts is favorable. Half-metal FMs (HMFs) were predicted,[13] and later on demonstrated by experiment,[14,15] to have close to 100% spin polarization of electrons, which is desirable for the contact FM material. With the ideal performance of spinFETs, it is further shown in Ref. 16, that nonvolatile memory and reconfigurable logic circuits can be constructed using these devices. Despite the theoretically predicted perfect spin polarization in the bulk HMF, there has been no observation of high spin polarized current injected from the HMF in experiments.[17] It is argued that when a HMF material contacts a nonmagnetic material, a randomization layer is formed at the interface[18] where spins of localized electrons are not aligned. This inevitable non-FM layer can decrease the injected polarization and reduce the MR ratio.[19]

Conduction mismatch between the FM and the semiconductor is another reason for the nonideal spin injection.[20] The solution was found in inserting a tunneling barrier between the FM and the semiconductor.[21,22] Even though the tunnel-

a)Electronic mail: gaoy@purdue.edu.

ing barrier resistance decreases the current, a significant enhancement of the injection efficiency is obtained. The third factor for nonideality of spinFET is spin scattering in the channel. In the presence of spin scattering, the two conducting channels (up-spin and down-spin) are mixed, which has a great impact on the carrier transport and the MR ratio. All these unavoidable imperfections of spinFETs should be taken into account when simulating the devices and assessing their performance potential.

An experimental prerequisite to building the spinFET is not just electrical injection of spin polarization in a semiconductor but also electrical detection of spin polarization.[23,24] Necessary conditions for efficient spin injection-detection and high MR have been determined theoretically.[22,25] One condition is low-resistance tunneling interface between the FM and a semiconductor. Low-resistance interface to silicon[26] and germanium[27] have been fabricated and characterized. A spinFET has been demonstrated only recently;[28] it contained HMF electrodes and was switched by the spin torque effect.

There have been a large number of theoretical and simulation studies on spin injection from FMs into semiconductors, see review.[29] Spin injection into semiconductors has been studied in a classical approximation, with drift-diffusion type of equations.[30] The nonequilibrium Green's function (NEGF) method[31] is a rigorous quantum transport treatment of nanoscale devices. First, the NEGF method has been applied in the research of MTJ devices.[32–35] A spinFET was treated by NEGF,[19] where the transport in the channel was considered as ballistic with scattering only at the source/drain and channel interfaces.

The present article reports the following advances compared to prior work: (1) simulation of spin-dependent quantum transport in a FM-semiconductor-FM structure, including tunneling barriers, (2) rigorous treatment of spin scattering, both in the channel and the randomization layer, (3) identification of realistic performance limits (especially MR) for spinFET with relevant factors of nonideality, and (4) implementation within a well established quantum transport simulator, nanoMOS.[36]

The rest of this paper is structured as follows. In Sec. II, we summarize the NEGF formalism used to describe the carrier transport in spinFETs and more specifically focus on the mathematical treatment of spin scattering and the physical connection with spin lifetime in various materials. In Sec. III, we apply this method to realistically structured spinFETs and quantitatively shows that the spin scattering affects the I-V characteristics and can dramatically reduce the MR ratio. The physical reasoning is then presented along with rigorous simulation results and two solutions to enhance the MR ratio are proposed and examined by numerical simulations. Finally, conclusions are drawn in Sec. IV.

II. NUMERICAL MODEL

The NEGF formalism is ideally suited for analyzing quantum transport of carriers in nanoscale devices. In this section we first briefly restate the main equations of the NEGF method necessary for understanding the results. For more details see the discussion in the previous studies.[31,37] Then we apply the NEGF approach to the spinFET with spin scattering. The key numerical model is described and the connection between the mathematical description and the physical model is discussed.

A. NEGF method

The channel material is described by a Hamiltonian matrix $[H]$ of size $N \times N$ blocks, N being the total number of grid points in the transport direction. Charging effects, which are a result of the interaction between carriers and the channel potential is incorporated via the potential matrix $[U]$. These serve as inputs in the equation for the retarded Green's function at a specific value of energy E

$$G(E) = [EI - H - U - \Sigma(E)]^{-1}. \tag{1}$$

The self-energy accounts for noncoherent processes and contains terms due to both contacts and due to scattering processes in the device

$$\Sigma(E) = \Sigma_L(E) + \Sigma_R(E) = \Sigma_S(E). \tag{2}$$

And similarly, the in- and out-scattering functions describing the change in populations of electrons and holes due to these incoherent processes are in the following expressions:

$$\Sigma^{\text{in/out}}(E) = \Sigma_L^{\text{in/out}}(E) + \Sigma_R^{\text{in/out}}(E) + \Sigma_S^{\text{in/out}}(E). \tag{3}$$

The spectral function $[A]$, related to the local density of states, and the electron/hole correlation functions $[G^{n/p}]$, which are proportional to the occupation numbers of electrons and holes in states of certain energy, are given by

$$A(E) = i[G(E) - G^{\dagger}(E)], \tag{4}$$

$$G^{n/p}(E) = G(E)\Sigma^{\text{in/out}}(E)G^{\dagger}(E). \tag{5}$$

These quantities are related to the local density of states, so they also satisfy the equation

$$A(E) = G^n(E) + G^p(E). \tag{6}$$

The strength of coupling to the left (source) and right (drain) contacts are described by the broadening matrices which are related to imaginary parts of the corresponding self-energy matrices

$$\Gamma_{L/R}(E) = i[\Sigma_{L/R}(E) - \Sigma_{L/R}^{\dagger}(E)]. \tag{7}$$

The in-scattering/out-scattering matrices represent the carrier injection and extraction rates into/out of the channel

$$\Sigma_{L/R}^{\text{in}}(E) = f_{L/R}(E)\Gamma_{L/R}(E), \tag{8}$$

$$\Sigma_{L/R}^{\text{out}}(E) = [1 - f_{L/R}(E)]\Gamma_{L/R}(E),$$

where $f_{L/R}(E)$ is the Fermi distribution functions in each contact.

Scattering, no matter if it is elastic or inelastic, can be visualized as the coupling of the channel and a reservoir.[31] The scattering process is physically described by the in-scattering/out-scattering matrices, which show the rate of

electrons coming into/out of a certain state. The sum of the two matrices gives the broadening matrix due to the scattering process

$$\Gamma_S(E) = \Sigma_S^{\text{in}}(E) + \Sigma_S^{\text{out}}(E), \tag{9}$$

from which the scattering-related self-energy can be obtained through a Hilbert transform as

$$\Sigma_S(E) = P\left[\int \frac{dE'\Gamma_S(E')}{2\pi(E-E')}\right] - i\frac{\Gamma_S(E)}{2}. \tag{10}$$

The imaginary part of $[\Sigma_S]$ obeys the same rule as that between $[\Gamma_{L/R}]$ and $[\Sigma_{L/R}]$. The real part of $[\Sigma_S]$ is obtained via the Hilbert transform, where P stands for the principal value of a singular integral, see Ref. 38 for details.

The NEGF and the Poisson equation are solved self-consistently, because the carrier density is obtained from the NEGF equations and used to solve for the electric potential, while the potential is necessary in order to solve the NEGF equations. The current is calculated once consistency is reached. This is the only loop necessary for the ballistic simulation (i.e., with zero scattering terms). In the scattering case, we have to consider an additional inner self-consistency loop to calculate the in-scattering or out-scattering matrix $[\Sigma_S^{\text{in/out}}]$ and the electron/hole correlation function $[G^{n/p}]$ in the NEGF formalism. As described in Refs. 31 and 37, the in-scattering/out-scattering energies $[\Sigma_S^{\text{in/out}}]$ contains $[G^{n/p}]$ as the inputs. They are used, in their turn, to calculate the contact self-energy $[\Sigma_S]$ through Eqs. (9) and (10), and consequently to obtain $[G]$ from Eq. (1). Once self-consistency in the inner loop is achieved, the iteration in the outer loop of NEGF and Poisson equations starts. One way to speed up the simulation is to bypass the computationally intensive Hilbert transform in Eq. (9). This is possible for elastic scattering, where the in-scattering/out-scattering functions depend on the Green's functions at the same value of energy only. In that case, the expression of the self-energy drastically simplifies, see Ref. 38. The spin scattering considered here is elastic, and thus, admits such a simplification. Thus, the expressions for the scattering terms become

$$\Sigma_S(E) = \mathbf{D}(E)G(E), \quad \Sigma^{\text{in}}(E) = \mathbf{D}(E)G^n(E), \tag{11}$$

$$\Sigma^{\text{out}}(E) = \mathbf{D}(E)G^p(E), \quad \Gamma(E) = \mathbf{D}(E)A(E),$$

where we introduced the scattering tensor $[\mathbf{D}]$. In this case, a simpler self-consistency loop is performed to calculate the Green's functions at separate values of energy, which proves to be less time consuming.

At node i of the grid, total current (I_i), and current for each energy level $[I_i(E)]$ are given by the summation over spin states and the integral over energies

$$\tilde{I}_i(E) = \sum_s \frac{ie}{\hbar}[H_{i,i+1}G^n_{i+1,i}(E) - H_{i+1,i}G^n_{i,i+1}(E)], \tag{12}$$

$$I_i = \int_{-\infty}^{+\infty} \frac{dE}{2\pi}\tilde{I}_i(E). \tag{13}$$

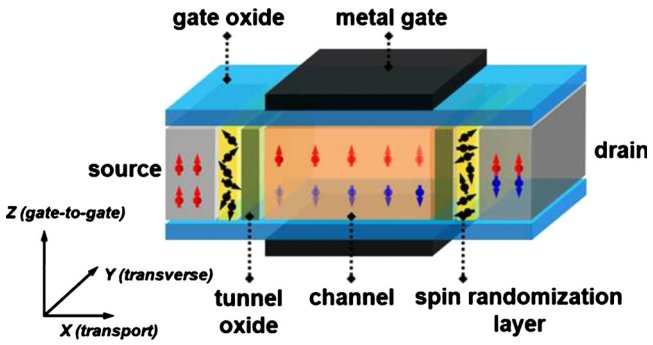

FIG. 1. (Color online) The spinFET schematic. The source and drain are HMF. The magnetization of the drain can be switched to obtain the parallel and antiparallel configurations of the two contacts. The double metal gates control the channel electrostatics. The source contact injects and the drain contact detects spin polarized current through oxide tunneling barriers. A spin randomization layer exists at the boundary of the HMF.

B. SpinFET description

The structure of the spinFET is illustrated in Fig. 1. Current flows along the transport direction x. Along the z direction are two metal gates separated by thin dielectric layers of gate oxide above and below the channel, which provide good electrostatics control. We have implemented the spin-dependent transport simulation based on the widely used simulator nanoMOS.[36] The width of the device in the transverse direction y is assumed to be large enough, so that the states with various transverse momentum (and corresponding energy E_y) can be analytically integrated, as it is implemented in nanoMOS, see Ref. 38 for details. Therefore, unless otherwise specified, energy E in the paper refers to the longitudinal energy due to motion along the x direction. In the example mostly used in this paper, the channel length is set at 12 nm, the channel thickness is 3 nm, and the thickness of both top and bottom gate oxides is 1 nm.

As the NEGF formalism is applied to spinFET, each element in the Hamiltonian $[H]$ is a 2×2 matrix, with the (1,1) element representing the onsite energy of "up"-spin state and the (2,2) element of the "down"-spin state, relative to a chosen preferred axis. Therefore, the resulting size of the Hamiltonian matrix $[H]$ is $2N\times2N$. The same is true for the contact self-energy $[\Sigma_{L/R}]$, whose elements are all zeros except for the top-left and the low-right 2×2 blocks. The nonzero elements in the contact self-energy describe the coupling of up-spin and down-spin carrier states in the source/drain and the channel

$$\begin{bmatrix} -te^{ik_{L/R,u}a} & 0 \\ 0 & -te^{ik_{L/R,d}a} \end{bmatrix}, \tag{14}$$

where $k_{L/R,u/d}$ is the momentum of the carrier in the source/drain in the up or down-spin state, and t is the amplitude of coupling between the source/drain and the channel. We assume that the magnetization of the contacts is along the same preferred axis; otherwise a transformation matrix has to be introduced in the above equation.[31] In the following analysis, the up-spin is set as the majority spin states and down-spin is the minority spin states in the source contact. If the magnetization of the contacts is parallel, the drain contact shares the same spin relation, whereas for the antiparallel case the

drain contact has exactly the opposite relation between up-down and majority-minority designation.

There are two important parameters of the FM contacts: the spin splitting Δ_S and the majority spin bandwidth E_ω. The spin splitting Δ_S is the energy difference between the bottom of the minority spin band and the bottom of the majority spin band. The majority spin bandwidth E_ω is defined as the energy difference between the Fermi level in the FM contact $E_{F,L/R}$ and the bottom of the majority spin band. If Δ_S is larger than E_ω, the FM is called a HMF. The Fermi level crosses just one spin band in such a material. Spin polarization close to 100% is expected in the material. But it does not necessarily translate into extremely high spin injection efficiency in the semiconductor. In our example we set the $\Delta_S = 2.5$ eV and $E_\omega = 2$ eV so that 100% spin injection can be achieved without the interface scattering. These values are close to the real case of the Δ_1 band in CoFeB, with the exception that the presence of other bands leads to less than 100% polarization.

We assume that the source and the drain are made of a HMF. The effects of nonideal spin polarization of carriers are accounted for by the spin randomization layer,[17,18] as shown in Fig. 1. It is a layer at the interface of a FM and semiconductor, where the spins of localized electrons are not aligned with the direction of magnetization but have random directions. The effect of the spin randomization layer is described as the first and the last block in the scattering self-energy $[\Sigma_S]$. The rest of the diagonal blocks in $[\Sigma_S]$ represent spin scattering in the channel, with, in general, different rates of scattering. This model would fairly well describe the effects of the typical FM contacts with ~50% spin polarization and even lower injection efficiency. The spin scattering in the channel, which is the main physics we intend to study here, has the similar effects on the device performance regardless of the contact materials, but the more realistic scenario of normal FM contacts without the spin randomization layers at the interface should be studied and will be the subject of future work.

The SB at the FM/semiconductor interface plays a vital role in spintronic transport.[26] It affects the spin injection and detection, and controls the performance of the devices. The SB is captured naturally in the NEGF formalism via the energy differences between the conduction bands in the semiconductor and in the metal.

The SB height of the FM/semiconductor interface in the conduction band is found to vary from 0.16 to 0.7 eV in MnAs/Si, CoFe/Si, and CoFeB/Si.[39] The SB height is very small (~0.02 eV) between CoFe and the valence band of Ge; and it varies with the insertion of a tunneling barrier.[40,41] In our simulation it is an input value that can be set to model different material combinations. We fix it at a relatively low value of 0.1 eV throughout the simulation and focus on the effect of the channel spin scattering on the device performance.

A tunneling oxide layer may be formed between the source/drain and the channel. It is modeled as a potential barrier of width W and energy height U_H, and the effective mass in the tunneling oxide is different from that in the channel. Since the tunneling barrier has a resistance that is spin-dependent, it is commonly used in ferro-MTJs to increase their MR.[4] Drift diffusion simulations[21] predict that the tunneling barrier with carefully adjusted resistance can increase the MR of a FM/semiconductor/FM stack as well. This effect exists for any tunneling barrier because different states within a band align close to the top of the barrier of up-spin and down-spin bands. It is especially pronounced, however, for certain tunneling barrier materials such as MgO.[42] In that case, up-spin and down-spin states over a certain range of energy belong to different bands with different crystal symmetries. Therefore they tunnel with drastically different probabilities. As a result, MgO additionally provides very efficient spin filtering effect and increases the spin polarization of the injected carriers. This effect can in principle be modeled by setting different height of the barrier or by different mass of carriers in the barrier for up-spin and down-spin electrons. In this paper we set different transport effective masses in the tunneling layer $m_{ox} = 0.378 m_0$ (corresponding to MgO as per Ref. 43) and in the channel $m_{ch} = 0.19 m_0$. The analytical integration over transverse (k_y) momenta is exact only in the case when the solution for the Green's function is independent on the transverse momentum, which is fulfilled for constant mass along the device. The integration is approximately valid for varying mass, if the current flows in the energy range (<0.1 eV) which is smaller than the characteristic potential differences in the device (~1 eV). We also assume a constant effective mass m_{ch} in the factor for the integration over the transverse momenta. The explicit form of the Green's functions and self energies with spin indices can be written as a set of diagonal blocks for each grid point

$$G = \begin{pmatrix} G_{uu} & G_{ud} \\ G_{du} & G_{dd} \end{pmatrix}, \quad \Sigma = \begin{pmatrix} \Sigma_{uu} & \Sigma_{ud} \\ \Sigma_{du} & \Sigma_{dd} \end{pmatrix}. \tag{15}$$

The in-scattering/out-scattering functions implement the spin scattering processes via the following relation to the electron/hole density $[G^{n/p}]$ and a scattering tensor $[\mathbf{D}]$, see Ref. 44

$$\Sigma_{S,ij}^{\text{in/out}}(E) = \sum_{kl} \mathbf{D}_{ijkl}^{n/p}(E) G_{kl}^{n/p}(E), \tag{16}$$

with $[\mathbf{D}]$ being the fourth-order tensors in spin indices at each grid point. The above equation can be qualitatively understood as the rate of electrons scattering into ($[\Sigma_S^{\text{in}}]$) or out of ($[\Sigma_S^{\text{out}}]$) the state with energy E being proportional to the existing electron ($[G^n]$) or hole ($[G^p]$) density. We assume here the same functional form for electrons $[\mathbf{D}^n]$ and holes $[\mathbf{D}^p]$. The scattering tensor can be separated into the coupling factor and the dimensionless tensor

$$\mathbf{D}(E) = D(E)\Phi. \tag{17}$$

For the case of isotropic scattering, the dimensionless tensor is[44]

$$4\Phi_{ij11} = \begin{pmatrix} 1 & 0 \\ 0 & 2 \end{pmatrix}, \quad 4\Phi_{ij12} = \begin{pmatrix} 0 & -1 \\ 0 & 0 \end{pmatrix}, \tag{18}$$

$$4\Phi_{ij21} = \begin{pmatrix} 0 & 0 \\ -1 & 0 \end{pmatrix}, \quad 4\Phi_{ij22} = \begin{pmatrix} 2 & 0 \\ 0 & 1 \end{pmatrix}$$

and the equation for the self-energy turns to,

$$\Sigma_s = \frac{D}{4}\begin{pmatrix} G_{uu} + 2G_{dd} & -G_{ud} \\ -G_{du} & 2G_{uu} + G_{dd} \end{pmatrix}. \tag{19}$$

To understand the scattering coupling factor D, we now relate it to the commonly used spin-flip time T_1 (or the scattering rate T_1^{-1}), which is more familiar to experimentalist.[4] The broadening function $\Gamma(E)$ is proportional to the spectral function $A(E)$ according to Eq. (11). On the other hand the broadening function is related to the spin-flip time

$$\Gamma(E) = \hbar\gamma(E) = \hbar/(2T_1). \tag{20}$$

For two-dimensional gas of carriers, density of states, and the spin-flip time do not change with energy. Since the density of states is calculated per unit area, and the spectral function is related to the unit cell of the grid, the relation between them is

$$g_{2D}(E) = \frac{m}{\pi\hbar^2} = \frac{2A(E)}{2\pi a_x a_y}. \tag{21}$$

Thus, we can express the coupling factor via the spin-flip time as in Ref. 38

$$D = \frac{\hbar^3}{2T_1 m a_x a_y}, \tag{22}$$

where a_x and a_y are the grid size in x and y directions and m is the mass of carriers. The spin-flip time can be related[21] to the spin diffusion length in a nondegenerate semiconductor with carrier density n and resistivity ρ

$$L_s = \sqrt{\frac{T_1 k_B T}{e^2 n\rho}}. \tag{23}$$

However, for a short channel device, the current is dominated by quantum resistance rather than resistivity of the channel. We will consider cases with widely varying rates of spin scattering. Expected spin-flip times for electrons are of the order of ~0.1 ns in silicon and ~1 ps in germanium. For holes, spin-flip times are comparable to momentum scattering times and can be as fast as ~1 fs. In the following, we will refer to carriers in the transistor as electrons. Our model can in principle be applied to holes, however, then one would need to include several valence bands in the semiconductor.

III. RESULTS

A. Coherent transport

Let us first consider the case of no spin scattering. In the spinFET studied in this paper, the source Fermi level lies between the majority (up-spin) and minority (down-spin) spin bands, with the parameters spin splitting Δ_S=2.4 and majority spin bandwidth E_ω=2.0, which agrees with theoretical calculation in Ref. 18. The energy difference of 0.4 eV between the Fermi level and the minority spin band is big enough to ensure that almost 100% of the injected electrons

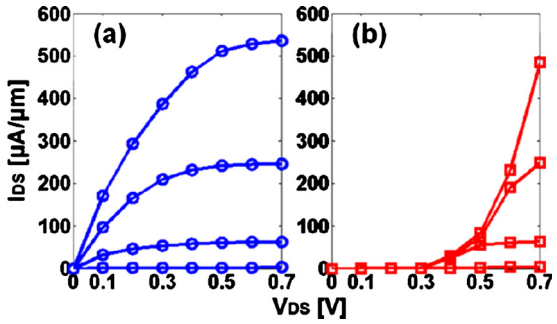

FIG. 2. (Color online) $I_{DS}-V_{DS}$ plots for (a) parallel and (b) antiparallel configurations in ballistic transport regime. The gate voltage values are 0.7, 0.5, 0.3, and 0.1 V, from top to bottom curves.

are up-spin. Absence of scattering will result in ballistic electron transport,[19] i.e., the current reaching the drain end is also 100% up-spin polarized without losing the spin and phase coherence. The electrons see different potential barriers for up-spin and down-spin in the drain contact of different magnetization configurations, and therefore, produce totally different I-V characteristics as shown in Fig. 2.

The up-spin channel is the only conducting channel in ballistic transport, and it has a high barrier potential in the drain contact under the antiparallel configuration which blocks the current flow and results in a very small drain current, as can be seen in Fig. 2(b) when $V_{DS}<0.4$ V. The voltage 0.4 V is called the turn-on voltage V_{ON} here, which is defined as the drain voltage required to push the minority spin band in the drain contact below the Fermi level of the source contact in the antiparallel configuration. When $V_{DS}>V_{ON}$, the up-spin band has states between the Fermi levels of source and drain; and the current will flow, as shown in Fig. 2(b) for $V_{DS}>0.4$ V.

The MR ratio plotted in Fig. 3 shows that with an ideal ballistic electron transport a high value of MR around 1000 can be obtained. The lower bound of V_{DS} is chosen in Fig. 3 to ensure the large MR ratio as well as a reasonable drive current of the spinFETs.

B. Scattering transport

Now let us consider the effects of spin scattering on the device performance. First, we introduce spin scattering in the channel only and leave out the spin randomization layer and

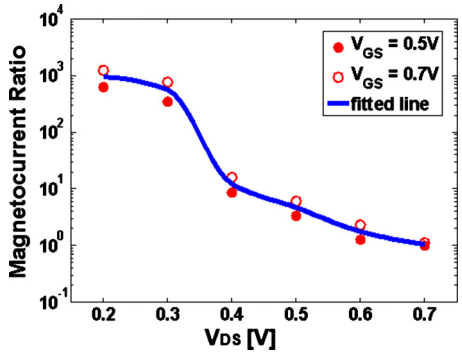

FIG. 3. (Color online) Magnetocurrent ratio of the ballistic spinFET under different drain bias. The dots are the data obtained as V_{GS}=0.5 or 0.7 V, and a fitted curve is plotted to represent the average values of the discrete dots.

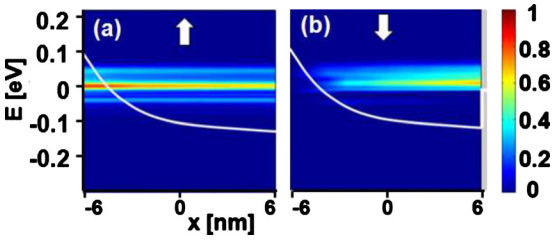

FIG. 4. (Color online) Energy-position resolved current in the channel for (a) up-spin and (b) down-spin in the parallel configuration. Up-spins convert to down-spins as the electrons traverse the device.

the tunneling barrier, as designated in Fig. 1. Suppose that 100% up-spin polarized electrons are injected into the channel. These electrons scatter for phonons or impurities with some probability and flip to the down-spin state as they travel along the channel. This scattering occurs everywhere inside the channel, as shown in Fig. 4. The closer the electron is to the drain, the higher probability it has to turn into down-spin. The amount of down-spin current increases with the increase in spin-flip coupling constant D. As can be seen in the following analysis, this large amount of down-spin electrons produced in the channel will cause current leakage into the drain and will degrade the device performance.

Spin scattering acts as a cause of shortened lifetime of electrons in the channel. In other words, the local density of state will spread out in real space and broaden in energy space as we increase the value D. This effect is observed in our simulation (Fig. 5) for different D which corresponding to different spin-flip times.

It is also seen in Fig. 5 that the band edge profiles inside the channel are different for these three values of D. It can be understood considering that electron distribution for both up-spin and down-spin electrons depends strongly on the spin-flip time, and thus, the modified charge density generates various potential energy profiles according to the Poisson equation. This dependence shows us the importance of a self-consistent solution of the NEGF and Poisson equation in the presence of the scattering in the channel. It is inaccurate to assume that the band profiles are the same with and without spin scattering. The charge distribution will affect the energy band and vice versa. The charge self-consistency can still be observed for different values of spin polarization, as shown in Fig. 6. The band profiles and the charge density (both up-spin and down-spin) in these two cases are influenced by

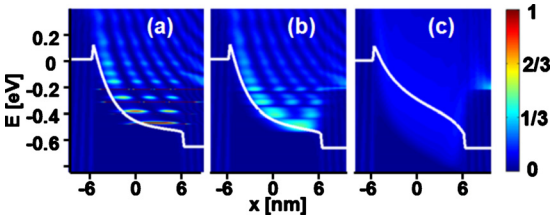

FIG. 5. (Color online) Energy-position resolved local density of state in the channel in parallel configuration. The spin-flip coupling constants D are 2.5×10^{-5} eV^2 in (a), 2.5×10^{-3} eV^2 in (b), and 1 eV^2 in (c), which corresponding to 40 ps, 0.4 ps, and 1 fs spin-flip times, respectively. The strong coupling reduces the spin-flip time, and also broadens the available states in the channel.

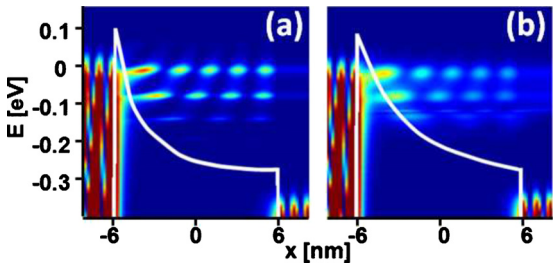

FIG. 6. (Color online) Energy-position resolved charge density in the channel in parallel configuration. The channel spin-flip coupling constants D and injection efficiencies are: 1×10^{-5} eV^2 (100 ps spin-flip time) and 90% in (a) and 1×10^{-2} eV^2 (0.1 ps spin-flip time) and 60% in (b). The energy band edge for up-spin is shown. It is obvious that the energy band edges and charge density are different in these two scenarios.

both interface and channel spin scattering. These two factors significantly affect the charge distribution in the device because different current and contact polarizations result in different injection and extraction rates for up-spin and down-spin electrons. Therefore, the process creates electrons pile-up in the channel. In another words, the charge self-consistent calculation is necessary in order to simulate the realistic performance of spinFETs with sensible values of the channel spin-flip time and the contacts polarization. From the above simulations, we observe that the spin scattering can: (1) flip the spin polarizations and create down-spin current along the channel, (2) broaden the local density of states, and (3) change the energy profile in the devices.

In addition to the above effects, spin scattering also affects MR of the spinFETs. Figure 7 shows that with spin scattering in the channel, the drain current in the antiparallel configuration increases dramatically even below the turn-on voltage [compare it to Fig. 2(b)].

Spin scattering induced leakage in the drain current can greatly decrease the MR of the devices, as shown in Fig. 8 for three different spin-flip coupling constants corresponding to spin-flip times of 1, 5, and 10 ps.

The peak in MR as a function of drain bias around V_{DS}=0.3 V is the result of a faster growth of I_{P} than that of I_{AP} at intermediate values of bias. The current in the parallel case, I_{P}, increases with V_{DS} bias almost linearly, like in a regular SB MOSFET [Fig. 7(a)]. For the antiparallel case [Fig. 7(b)], current I_{AP} at lower bias V_{DS}, mainly consists of

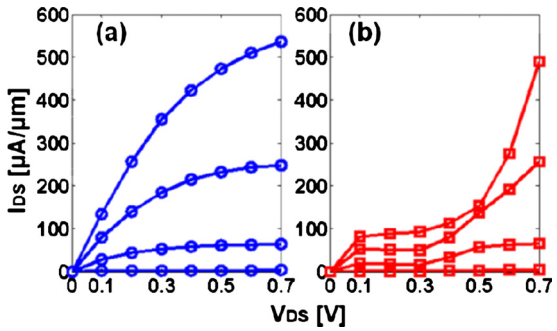

FIG. 7. (Color online) $I_{DS}-V_{DS}$ plots for (a) parallel and (b) antiparallel configurations in scattering transport regime. The gate voltage values are 0.7, 0.5, 0.3, and 0.1 V, from top to bottom curves. The spin-flip coupling constant is 10^{-3} eV^2, which corresponds to 1 ps spin-flip time in the channel.

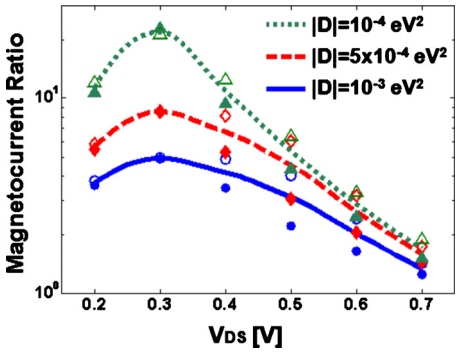

FIG. 8. (Color online) Magnetocurrent ratio of spinFETs with spin scattering under different drain bias and with different spin-flip coupling constants. The symbols are for simulation results at V_{GS}=0.5 V (solid) or 0.7 V (open) and fitted curves are plotted to represent the median values of the two cases.

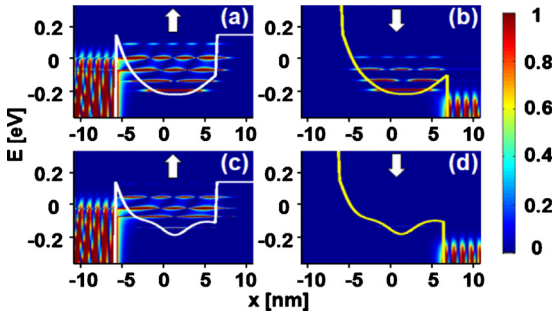

FIG. 10. (Color online) Energy-position resolved charge density of up-spin [(a) and (c)] and down-spin [(b) and (d)] current, for scattering [(a) and (b)], and ballistic [(c) and (d)] transport regimes. In the scattering transport regimes, the up-spins turn to down-spins and escape to the drain, while no down-spins current flows in the ballistic case.

the minority spin current that occurs due to the spin-flip scattering. This is confirmed by the fact that such current in the antiparallel state is not observed in the ballistic case [Fig. 2(b)]. At very small V_{DS}(<0.1 V) it increases linearly, as shown in Figs. 7(a) and 9(b), but then saturates due to the limited amount of electrons experiencing scattering in the energy range where current flows. Further increasing the V_{DS} to 0.4 V increases the energy range where current can flow, but due to quantum confinement in the channel, only an energy shift in the minority current maxima and no noticeable increase in the current magnitude are observed, as in Figs. 7(b) and 9(b). This causes a plateau in the function of current vs. bias. As V_{DS} increases from 0.4 to 0.7 V, the energy range opens for the majority current, and the total I_{AP} increases dramatically thanks to the large amount of up-spin current, as seen in Figs. 7(b) and 9(c). The peak of MR occurs at the plateau of I_{AP} at V_{DS}=0.3 V in this case.

Figure 9 separately plots up-spin and down-spin currents in the antiparallel configuration for both ballistic and scattering cases with the bias condition $V_{GS}=V_{DD}$=0.7 V and V_{DS}=0.2 V. Before the device is turned on ($V_{DS}<V_{ON}$ =0.4 V) and without spin scattering, almost 100% up-spin electrons injected from the source are confined in the quantum well formed by the channel and cannot escape into the drain [Fig. 10(c)]. The negligible down-spin current flows freely from source to the drain but contributes very little to overall current [Fig. 10(d)]. When spin scattering is turned on, a large amount of down-spin electrons is generated [Fig. 10(b)]. They escape to the drain contact thanks to the low barrier between the channel and the drain. The up-spin electrons remain confined in the channel as in Fig. 10(a). Note that in the up-spin quantum well, the electrons occupy certain eigenstates of energy. One can notice the five lowest modes that contain from one to five antinodes of the wave function, respectively [Figs. 10(a) and 10(c)]. The energy states are wider in the case shown in Fig. 10(a) than in Fig. 10(c), because of the above mentioned spin-flip coupling constant values.

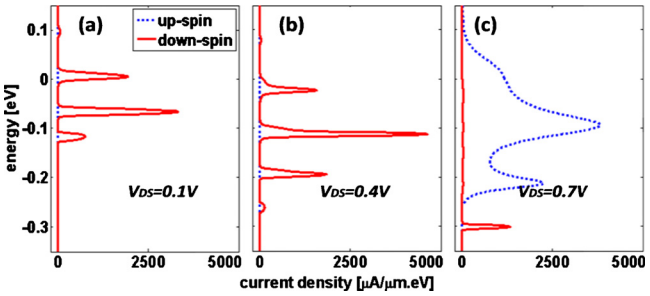

FIG. 9. (Color online) Current-energy plot in antiparallel configuration for up-spin (majority, solid line) and down-spin (minority, dashed line) current at different V_{DS} as V_{GS}=0.7 V. Very small amount of current increase is seen as V_{DS} increase from 0.1 to 0.4 V [(a) to (b)]. A large amount of up-spin current flows as V_{DS} rises past 0.3 V as in (c).

The interface spin randomization layer can also have the same effect as the channel scattering and be detrimental to the MR ratio. It has been found in the previous work that the interface treatment at the drain side is more pertinent to achieving high MR ratio.[19] With an estimate for the coupling constant D=1 eV^2 and a very high spin injection polarization ~80%, the MR ratio drops drastically compared to the ideal case without the spin randomization layers, as indicated in Fig. 11.

The spin randomization layer, also called "magnetically dead layer," does physically exist as an amorphous layer at the FM/semiconductor interface.[45] A theory—experiment coupled study[46] also suggests that the spin current could polarize the localized spins within the magnetically dead layer and has a transient effect on the terminal current. Therefore,

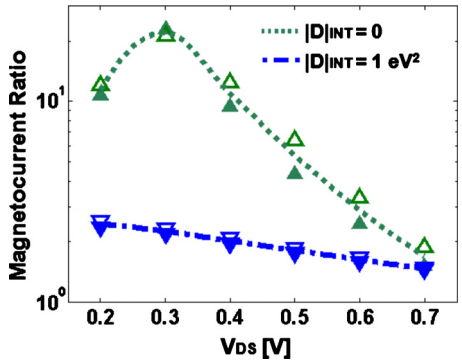

FIG. 11. (Color online) Magnetocurrent ratio of the spinFETs with spin scattering and interface spin scattering under different drain bias and with different interface spin-flip coupling constants. The channel spin-flip coupling is 10^{-4} eV^2 (10 ps spin-flip time). The symbols are for simulation results at V_{GS}=0.5 V (solid) or 0.7 V (open) and fitted curves are plotted to represent the median values of the two cases.

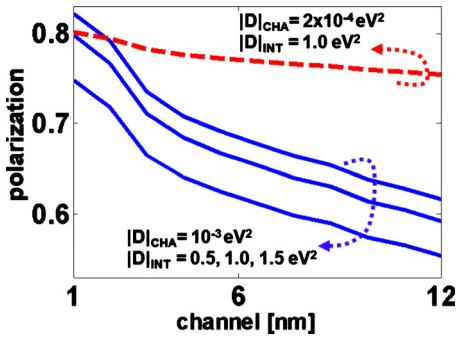

FIG. 12. (Color online) Spin polarization along the channel with different interface spin-flip coupling constant D_{INT} and same channel scattering constant D_{CHA} (solid line). The empirical parameter D_{INT} adjusts the spin injection efficiency, while D_{CHA} controls the spin scattering along the channel.

it is important to understand the physics of this layer and how it affects the device performance. As it is already known that this layer will randomize the injection spin, in our simulation this layer is modeled with an empirical parameter known as the interface spin-flip coupling constant D_{INT}, which describes the coupling strength of the electron spins and localized spins. This tunable parameter can be adjusted to achieve different spin injection efficiencies. It is also assumed in this work that the localized spins are invariable and always quickly return to equilibrium after scattering with electrons. Some experiments[47] result in estimates of injection efficiency around 30%–50%, which was used to benchmark the interface spin-flip coupling constant in our simulation. As shown in Fig. 12, the interface scattering tensor D_{INT} controls injection efficiency, and the channel scattering tensor D_{CHA} affects the spin dephasing along the channel. Therefore, the combination of these two parameters can be used to model the realistic spin polarization scenario of spinFETs.

In order to improve the MR ratio, the current in the parallel configuration should be maximized and the current in the antiparallel configuration should be minimized. In the parallel configuration the down-spin channel is not conductive with or without spin scattering, because the band edge profile contains a high potential wall at the drain end. The

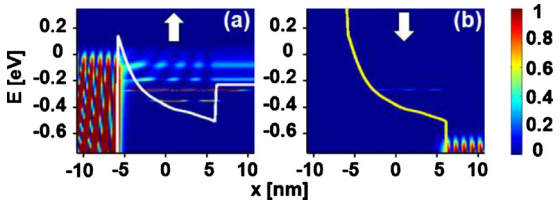

FIG. 14. (Color online) Energy-position resolved charge density of the (a) up-spin and the (b) down-spin current in the scattering transport at the on-state in the antiparallel configuration. The high V_{DS} pushes down the drain energy band, which gives a large amount of up-spin current flowing out of drain.

up-spin electron transport is similar to that in a SB FET. The comparison of Figs. 2(b) and 7(b) stresses the need to decrease the current in the antiparallel configuration as the only way to improve the MR ratio. The magnitudes of up-spin and down-spin current in parallel and antiparallel configurations are plotted in Fig. 13.

The subplots (a) and (b) verify the dominance of the up-spin current in the parallel configuration even at relatively high spin-flip coupling (spin-flip time of ~1 ps). The antiparallel up-spin current increases to almost 600 $\mu A/\mu m$ in the on-state as seen in Fig. 13(c), which can be explained with the help of the energy-position resolved charge density plot in Fig. 14. In the on-state with $V_{GS}=V_{DS}=V_{DD}=0.7$ V, the high gate bias creates a thin SB between the source and the channel, permitting a large amount of electrons to tunnel through. The high drain bias ensures that the bottom of the minority electron conduction band in the drain is below the source Fermi level; and, therefore, large current flows. Below the turn-on voltage ($V_{DS}<V_{ON}$), however, down-spin current due to spin scattering is much larger [Fig. 13(d)] than the up-spin current limited by the quantum well confinement, as seen in Fig. 10(b). Thus the up-spin current dominates the total current in the on-state of the spinFETs, and the down-spin current dominates in the off-state.

To decrease the high antiparallel current, two solutions are considered here. The first one is to reduce the up-spin current at $V_{DS}>V_{ON}$ by increasing the spin splitting Δ_S in the

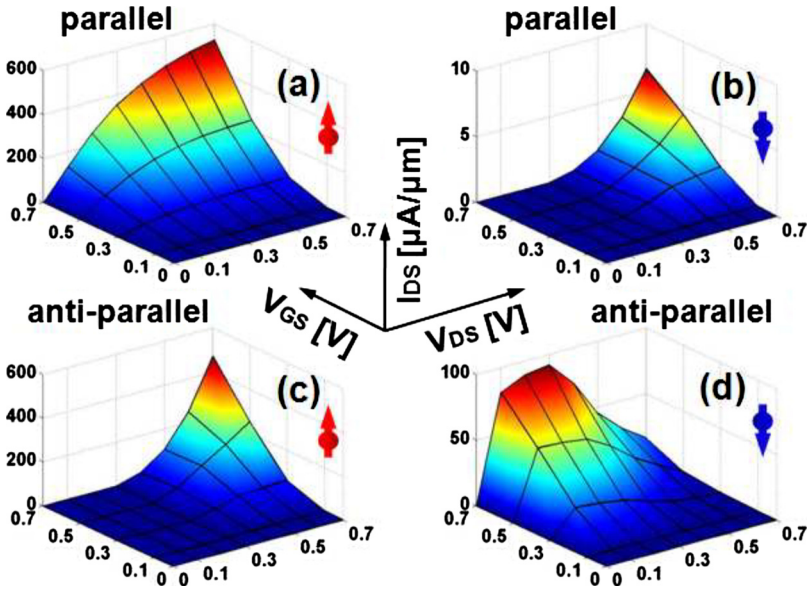

FIG. 13. (Color online) $I_{DS}-V_{DS}$, V_{GS} plots of up-spin [(a) and (c)] and down-spin [(b) and (d)] current, for parallel [(a) and (b)], and antiparallel configuration [(c) and (d)]. The spin-flip coupling ($|D|=10^{-3}$ eV^2) gives large up-spin current at the on-state and large down-spin current at medium V_{DS} in the antiparallel configuration.

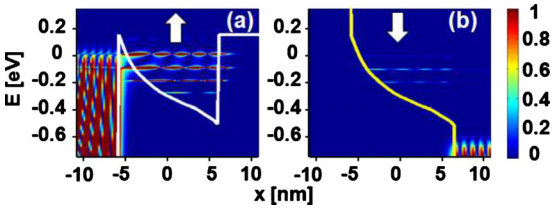

FIG. 15. (Color online) Energy-position resolved charge density of the (a) up-spin and the (b) down-spin current in the scattering regime at the on-state. The source and drain are antiparallel configured. The high V_{DS} pushes down the drain energy band, but the large spin splitting blocks the electrons from going into the drain, which reduces the current at the on-state.

drain contact. The band diagram and charge density are plotted in Fig. 15. The large Δ_S presents a high potential wall to electrons arriving at the drain and thereby blocks the current. The simulation indicates that the up-spin current is reduced from 560 to 0.6 $\mu A/\mu m$ at the same bias conditions. This is due to the fact that the quantum well confines the up-spin electrons in the channel, increasing the probability of spin scattering into down-spin states. Therefore, more down-spin electrons are generated in the case of a larger Δ_S in the drain and the down-spin current increases from 7 to 57 $\mu A/\mu m$ [Figs. 14(b) and 15(b)]. But the total current drops as a result of the dramatic decrease in the up-spin current.

The second method is to reduce the down-spin current at $V_{DS} < V_{ON}$ by inserting a tunneling barrier between channel and drain. The high antiparallel leakage down-spin current at $V_{DS} < V_{ON}$ induced by spin scattering is the main cause of low MR ratio [Fig. 16(b)]. The tunneling potential barrier effectively blocks the current and diminishes the leakage, as shown in Fig. 16(a). We simulate a 4 nm thick spin-dependent tunneling barrier that exhibits a higher barrier height for down-spin and a low barrier height for up-spin electrons. In the parallel configuration, the up-spin dominated current changes insignificantly, while the down-spin leakage current in antiparallel configuration is lower. The effect of the spin-dependent tunneling oxide is exhibited at both source and drain ends. The barrier at the source end can filter the injected current and increase its polarization, and the barrier at the drain end can stop the leakage down-spin current below the turn-on voltage and almost eliminate the current in the antiparallel configuration. Thus the MR ratio is $\sim 50\times$ higher with the spin selective tunneling oxide than without it.

The enhancement of MR ratio by adding the tunneling barriers can be seen in Fig. 17. In the on-state that V_{GS}

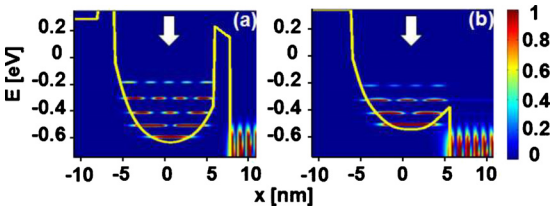

FIG. 16. (Color online) Energy-position resolved charge density of the down-spin current in the scattering regime. The source and drain are antiparallel configured. The tunneling barrier for the down-spin electrons between the channel and drain can lower the total current and, therefore, increase MR by about 50×.

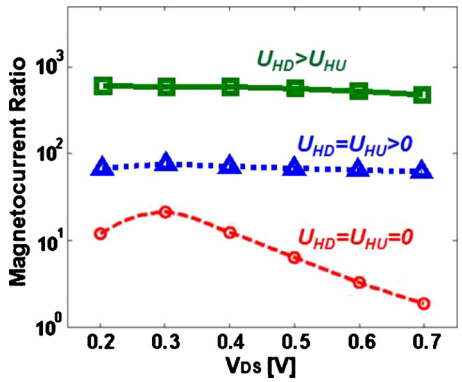

FIG. 17. (Color online) Magnetocurrent ratio of the spinFETs with various tunneling barriers configurations under different drain bias. The tunneling barriers in the source and drain ends are of 4 nm thick and 0.6 eV high. There are three devices simulated here: without tunneling barriers for both up- and down-spins (dashed line), with the same tunneling barriers for both spins (dotted line), and with the different barriers for both spins (solid line).

$= V_{DD} = 0.7$ V, the spinFETs without the tunneling barriers have a low MR of ~20. It can reach 80 with the insertion of the same barriers ($U_{HD} = U_{HU}$) for both up- and down-spins. In the case that the tunneling barrier for the down-spin is higher than that for the up-spin electrons ($U_{HD} > U_{HU}$), the MR can increase to ~500.

IV. CONCLUSION

In this work we have demonstrated a rigorous quantum transport (NEGF) simulation of spinFETs taking into account spin scattering, tunneling and SBs, and self-consistent charge distribution. In the ideal case without channel scattering the device shows very large MR ratio of the order of 10^3. Spin scattering generates a large amount of down-spin electrons, which increases the current in the antiparallel configuration, and eventually, degrades the MR ratio to around 10 with a reasonable assumption for the spin-flip time in a semiconductor. The MR ratio becomes even lower when the inevitable spin randomization layer at the FM/semiconductor interface is included. As a result of our numerical study, two solutions are proposed to improve the performance of spinFETs. The first method is to increase the energy spin splitting in the drain contact in order to create a high potential barrier to block the drain leakage current, which mainly consists of the up-spin electrons coming from the source. Another solution is to insert a spin-selective tunneling oxide layer between the source/drain and the channel, which brings the MR ratio up to ~500.

ACKNOWLEDGMENTS

The authors gratefully acknowledge the support of the Nanoelectronic Research Initiative through a supplement to the Network for Computational Nanotechnology. We express our appreciation for the helpful discussions with Supriyo Datta of Purdue University, Brian Doyle and George Bourianoff of Intel.

[1]Semiconductor Industry Association, International Technology Roadmap for Semiconductors, Chapter, "Emerging research devices," 2009, http://public.itrs.net/

[2]S. A. Wolf, D. D. Awschalom, R. A. Buhrman, J. M. Daughton, S. von Molnar, M. L. Roukes, A. Y. Chtchelkanova, and D. M. Treger, Science **294**, 1488 (2001).
[3]A. Fert, Rev. Mod. Phys. **80**, 1517 (2008).
[4]I. Žutić, J. Fabian, and S. D. Sarma, Rev. Mod. Phys. **76**, 323 (2004).
[5]M. N. Baibich, J. M. Broto, A. Fert, F. Nguyen Van Dau, F. Petroff, P. Etienne, G. Creuzet, A. Friederich, and J. Chazelas, Phys. Rev. Lett. **61**, 2472 (1988).
[6]G. Binasch, P. Grünberg, F. Saurenbach, and W. Zinn, Phys. Rev. B **39**, 4828 (1989).
[7]S. S. P. Parkin, C. Kaiser, A. Panchula, P. M. Rice, B. Hughes, M. Sament, and S. Yang, Nature Mater. **3**, 862 (2004).
[8]E. B. Myers, D. C. Ralph, J. A. Katine, R. N. Louie, and R. A. Buhrman, Science **285**, 867 (1999).
[9]S. Sugahara and M. Tanaka, Appl. Phys. Lett. **84**, 2307 (2004).
[10]B. Huang, D. J. Monsma, and I. Appelbaum, Phys. Rev. Lett. **99**, 177209 (2007).
[11]S. S. P. Parkin, K. P. Roche, M. G. Samant, P. M. Rice, R. B. Beyers, and R. E. Scheuerlein, J. Appl. Phys. **85**, 5828 (1999).
[12]S. Datta and B. Das, Appl. Phys. Lett. **56**, 665 (1990).
[13]R. A. de Groot, F. M. Mueler, P. G. van Eugen, and K. H. J. Buschow, Phys. Rev. Lett. **50**, 2024 (1983).
[14]R. B. Mancoff, B. M. Clemens, E. J. Singley, and D. N. Basov, Phys. Rev. B **60**, R12565 (1999).
[15]K. Inomata, N. Ikeda, N. Tezuka, R. Goto, S. Sugimoto, M. Wojcik, and E. Jedryka, Sci. Technol. Adv. Mater. **9**, 014101 (2008).
[16]M. Tanaka and S. Sugahara, IEEE Trans. Electron Devices **54**, 961 (2007).
[17]C. T. Tanaka, J. Nowak, and J. S. Moodera, J. Appl. Phys. **86**, 6239 (1999).
[18]G. A. de Wijs and R. A. de Groot, Phys. Rev. B **64**, 020402 (2001).
[19]T. Low, M. S. Lundstrom, and D. E. Nikonov, J. Appl. Phys. **104**, 094511 (2008).
[20]G. Schmidt, D. Ferrand, and L. W. Molenkamp, Phys. Rev. B **62**, R4790 (2000).
[21]E. I. Rashba, Phys. Rev. B **62**, R16267 (2000).
[22]A. Fert and H. Jaffrès, Phys. Rev. B **64**, 184420 (2001).
[23]H. C. Koo, H. Yi, J.-B. Ko, J. Chang, S.-H. Han, D. Jung, S.-G. Huh, and J. Eom, Appl. Phys. Lett. **90**, 022101 (2007).
[24]X. Lou, C. Adelmann, S. A. Crooker, E. S. Garlidi, J. Zhang, K. S. Madhukar Reddy, S. D. Flexner, C. J. Palmstrøm, and P. A. Crowell, Nat. Phys. **3**, 197 (2007).
[25]W. Van Roy, P. Van Dorpe, R. Vanheertum, P.-J. Vandormael, and G. Borghs, IEEE Trans. Electron Devices **54**, 933 (2007).
[26]B.-C. Min, K. Motohashi, C. Lodder, and R. Jansen, Nature Mater. **5**, 817 (2006).
[27]Y. Zhou, M. Ogawa, M. Bao, W. Han, R. K. Kawakami, and K. Wang, Appl. Phys. Lett. **94**, 242104 (2009).
[28]T. Marukame, T. Inokuchi, M. Ishikawa, H. Sugiyama, and Y. Saito, Tech. Dig. - Int. Electron Devices Meet. **2009**, 09-2.
[29]A. M. Bratkovsky, Rep. Prog. Phys. **71**, 026502 (2008).
[30]I. Zutić, J. Fabian, and S. C. Erwin, IBM J. Res. Dev. **50**, 121 (2006).
[31]S. Datta, *Quantum Transport: Atom to Transistor* (Cambridge University Press, Cambridge, 2005).
[32]A. A. Yanik, G. Klimeck, and S. Datta, Phys. Rev. B **76**, 045213 (2007).
[33]S. Salahuddin, D. Datta, P. Srivastava, and S. Datta, Tech. Dig. - Int. Electron Devices Meet. **2007**, 121.
[34]X.-G. Zhang and W. H. Butler, Phys. Rev. B **70**, 172407 (2004).
[35]D. Waldron, L. Liu, and H. Guo, Nanotechnology **18**, 424026 (2007).
[36]Z. Ren, S. Goasguen, A. Matsudaira, S. S. Ahmed, K. Cantley, and M. Lundstrom, nanoMOS, 2006. Available online at: https://www.nanohub.org/tools/nanomos/
[37]M. P. Anantram, M. S. Lundstrom, and D. E. Nikonov, Proc. IEEE **96**, 1511 (2008).
[38]D. E. Nikonov, G. I. Bourianoff, and P. A. Gargini, http://nanohub.org/resources/7772
[39]K. Sugiura, R. Nakane, S. Sugahara, and M. Tanaka, Appl. Phys. Lett. **89**, 072110 (2006).
[40]D. Lee, S. Raghunathan, R. J. Wilson, D. E. Nikonov, K. Saraswat, and S. X. Wang, Appl. Phys. Lett. **96**, 052514 (2010).
[41]Y. Zhou, W. Han, Y. Wang, F. Xiu, J. Zou, R. K. Kawakami, and K. L. Wang, Appl. Phys. Lett. **96**, 102103 (2010).
[42]W. H. Butler and A. Gupta, Nature Mater. **3**, 845 (2004).
[43]W. H. Butler, X.-G. Zhang, T. C. Schulthess, and M. J. MacLaren, Phys. Rev. B **63**, 054416 (2001).
[44]S. Datta, Proceedings of the International School of Physics "Enrico Fermi" Course CLX edited by A. D'Amico, G. Balestrino, and A. Paoletti, (IOS Press, Amsterdam and SIF Bologna, 2005), p. 244.
[45]J. S. Tsay, C. S. Yang, Y. Liou, and Y. D. Yao, J. Appl. Phys. **85**, 4967 (1999).
[46]D. Saha, L. Siddiqui, P. Bhattacharya, S. Datta, D. Basu, and M. Holub, Phys. Rev. Lett. **100**, 196603 (2008).
[47]B. Huang, L. Zhao, D. J. Monsma, and I. Appelbaum, Appl. Phys. Lett. **91**, 052501 (2007).